A COMPILATION OF CHARGED-PARTICLE INDUCED THERMONUCLEAR REACTION RATES

C. Angulo[1], M. Arnould, and M. Rayet[2],
Institut d'Astronomie et d'Astrophysique CP226,
Université Libre de Bruxelles, B-1050 Bruxelles, Belgium,

P. Descouvemont[3], D. Baye, and C. Leclercq-Willain,
Physique Nucléaire Théorique et Physique Mathématique CP229,
Université Libre de Bruxelles, B-1050 Bruxelles, Belgium,

A. Coc, S. Barhoumi[4], and P. Aguer[5],
Centre de Spectrométrie Nucléaire et Spectrométrie de Masse,
IN2P3-CNRS, F-91405 Orsay, France,

C. Rolfs,
Experimentalphysik III, Ruhr-Universität Bochum,
D-44780 Bochum, Germany,

R. Kunz, J. W. Hammer, and A. Mayer,
Institut für Strahlenphysik, Universität Stuttgart,
D-70550 Stuttgart, Germany,

T. Paradellis, S. Kossionides, C. Chronidou, and K. Spyrou,
Laboratory for Material Analysis, Institute of Nuclear Physics,
N.C.S.R Demokritos,
GR-15310 Aghia Paraskevi, Greece,

S. Degl'Innocenti[6], G. Fiorentini, B. Ricci, and S. Zavatarelli[7],
Dipartimento di Fisica, Universita di Ferrara and INFN-Ferrara,
I-44100 Ferrara, Italy,

C. Providencia[8], H. Wolters[9], and J. Soares,
Centro de Física Nuclear, Universidade de Lisboa,
P-1699 Lisboa Cedex, Portugal,

C. Grama,
Institute of Physics and Nuclear Engineering,
P.O. Box MG-6, Bucharest, Romania,

J. Rahighi[10], A. Shotter, and M. Lamehi Rachti[10],
Department of Physics and Astronomy, University of Edinburgh,
EH9-3JZ Edinburgh, United Kingdom.

[1] Present address: Institut de Physique Nucléaire, Université catholique de Louvain, B-1348 Louvain-la-Neuve, Belgium.
[2] Chercheur qualifié FNRS
[3] Directeur de Recherches FNRS
[4] Permanent address: Institut de Physique, USTHB, B.P. 32, El-Alia, Bab Ezzouar, Algiers, Algeria.
[5] Present address: CENBG, IN2P3-CNRS, et Université de Bordeaux I, F-33175 Gradignan, France.
[6] Permanent address: Dipartimento di Fisica, Universita di Pisa, I-56100 Pisa, Italy.
[7] Permanent address: Dipartimento di Fisica, Universita di Genova and INFN-Genova, I-16146 Genova, Italy.
[8] Permanent address: Centro de Física Teórica, Universidade de Coimbra, P-3000 Coimbra, Portugal.
[9] Permanent address: Escola Superior de Ciencias e Tecnologia, Universidade Católica Portuguesa, P-3080 Figueira da Foz, Portugal.
[10] Permanent address: Van De Graaff Laboratory, Nuclear Research Centre, Atomic Energy Organisation of Iran, 14376 Tehran, Iran.

Abstract

Low-energy cross section data for 86 charged-particle induced reactions involving light ($1 \leq Z \leq 14$), mostly stable, nuclei are compiled. The corresponding Maxwellian-averaged thermonuclear reaction rates of relevance in astrophysical plasmas at temperatures in the range from 10^6 K to 10^{10} K are calculated. These evaluations assume either that the target nuclei are in their ground state, or that the target states are thermally populated following a Maxwell-Boltzmann distribution, except in some cases involving isomeric states.

Adopted values complemented with lower and upper limits of the rates are presented in tabular form. Analytical approximations to the adopted rates, as well as to the inverse/direct rate ratios, are provided.

1 INTRODUCTION

Since the fifties, astrophysics has advanced at a remarkable pace, and has achieved an impressive record of success. One of the factors contributing to these rapid developments is without any doubt a series of spectacular breakthroughs in *Nuclear Astrophysics*, which embodies the special interplay between nuclear physics and astrophysics.

The close relationship between these two major scientific disciplines comes about because of the clear demonstration that the structure, evolution and composition of a large variety of cosmic objects, including the Solar System, bear strong imprints of the properties of atomic nuclei, as well as of their interactions. In such conditions, careful and dedicated experimental and theoretical studies of a large variety of nuclear processes are indispensable tools for the modeling of ultra-macroscopic systems such as stars.

Thanks to the impressive skill and painstaking efforts of nuclear physicists involved in astrophysics, remarkable progress has been made over the years in order to evaluate reaction cross sections at energies that are as close as possible to those of astrophysical relevance. This is a highly challenging task indeed: for charged particle reactions, the energies of interest are much lower than the Coulomb barrier height, and the cross sections to be determined are among the smallest ones ever measured in the laboratory. The experimental problems nuclear physics has to face through astrophysics are even more severe as the properties and cross sections of a large variety of exotic (neutron-deficient or neutron-rich) nuclei are needed in some astrophysical modelings. The radioactive ion beam facilities in operation in some countries have already made some interesting data available. In a near future, many such facilities now under development all over the world will bring a wealth of new data of astrophysical interest.

In spite of much experimental effort and achievement, it is evident that nuclear models have to bring a substantial share to the evaluation of nuclear reaction rates in astrophysical plasmas. Theory has indeed (i) to provide as reliable extrapolations of experimental data as possible to low-energy regions of astrophysical relevance where this information is generally lacking, (ii) to extract purely nuclear effects from low-energy experimental data that may be "polluted" by atomic (screening) effects, or (iii) to provide reaction rates on excited nuclear states that are thermally populated in astrophysical conditions, or on nuclei away from the valley of nuclear stability. These situations are not amenable to experiments at the present time, and will remain so for a long time to come.

Because of its very success and growth, in particular through the impressive achievements in experimental and theoretical nuclear physics mentioned above, nuclear astrophysics faces in fact a new and difficult challenge. The rapidly growing wealth of nuclear data becomes less and less easily accessible to the astrophysics community. Mastering this volume of information and making it available in an accurate and usable form for incorporation into stellar evolution or nucleosynthesis models become urgent goals of prime necessity. The establishment of the required level in the privileged communication between nuclear physicists and astrophysicists makes necessary the build-up of well documented and evaluated sets of experimental data or theoretical predictions of astrophysical relevance.

This has been the driving motivation for the setting-up in 1993 of a network of nuclear physics and astrophysics laboratories from Belgium, France, Germany, Greece, Italy, Portugal and the United Kingdom under the *Human Capital and Mobility* (HCM) Programme of the European Commission, this consortium being coordinated by the Institut d'Astronomie et d'Astrophysique of the Université Libre de Bruxelles. The aim of this collaborative effort is to provide a detailed evaluation and compilation of the rates for an ensemble of charged particle induced nuclear reactions on *stable* targets up to Silicon. Also included are several reactions on the unstable nuclei ^{7}Be, ^{13}N, ^{22}Na and ^{26}Al of special astrophysical significance. This work is meant to supersede the only compilation of such reactions for astrophysical purposes issued by W.A. Fowler and collaborators [FO67, FO75, HA83, CA85, CA88] (recent works give recommended values for the cross section of solar fusion reactions only [CA97, AD98]). The main innovative features with respect to this compilation that have been of constant concern during our work may be summarized as follows:

(1) detailed references are provided to the sources of the basic data (cross sections, resonance energies, spins, parities,...) that are necessary in order to calculate the rates;
(2) the way these data have been evaluated is documented to a substantial extent;
(3) uncertainties have been analyzed in detail in order to provide realistic lower and upper bounds to the adopted rates;
(4) the evaluated/compiled rates are provided in tabular form. This format is considered to be especially well suited to modern computer use (as in the opacity tables [RO92]). However, analytical formulae approximating the rates might be wanted by some users, and have also been established.

Section 2 describes the formalism that has been adopted in order to derive the astrophysical rates of the charged particle induced reactions and of their reverse. In addition to the general formulae used for the calculation of the Maxwellian-averaged reaction rates, it contains a description of the data treatment, as well as the selected analytical expressions approximating the reaction rates. Section 3 explains the format adopted for the presentation of the results. Table I displays all the compiled reactions. Short write-ups are provided in Table II for the 86 reactions that have been analyzed. Analytical approximations of the reaction rates and the partition functions are given in Table III and IV, respectively. More details are available electronically on the web site http://pntpm.ulb.ac.be/nacre.htm.

2 GENERAL FORMALISM

2.1 Calculation of Maxwellian-averaged reaction rates $N_{\rm A}\langle\sigma v\rangle$

Here, as well as in Sects. 2.2-2.4, all equations apply to target nuclei in their ground state. Questions related to the thermal excitation of the targets are considered explicitly in Sects. 2.5 and 2.6. We refer to Appendix A for the meaning of symbols and for the units used implicitly in some of the following formulae.

2.1.1 General definitions

For two-body reactions, the Maxwellian-averaged reaction rates $N_{\rm A}\langle\sigma v\rangle$ are computed from [FO67]

$$N_{\rm A}\langle\sigma v\rangle \;=\; N_{\rm A}\,\frac{(8/\pi)^{1/2}}{\mu^{1/2}(k_{\rm B}T)^{3/2}}\int_0^\infty \sigma E\exp(-E/k_{\rm B}T)\;dE, \tag{1}$$

where $N_{\rm A}$ is the Avogadro number, μ the reduced mass of the system, $k_{\rm B}$ the Boltzmann constant, T the temperature, σ the cross section, v the relative velocity, and E the energy in the centre-of-mass system. The only three-body reactions considered in this compilation are ^{4}He(αn,γ)^{9}Be and ^{4}He($\alpha\alpha,\gamma$)^{12}C. The formulae to be applied in these cases are explained in the corresponding comments of Table II.

When $N_{\rm A}\langle\sigma v\rangle$ is expressed in cm^3 mol^{-1} s^{-1}, the energies E and $k_{\rm B}T$ in MeV, and the cross section σ in barn, Eq. (1) leads to

$$N_{\rm A}\langle\sigma v\rangle \;=\; 3.7313\times10^{10}\;A^{-1/2}\,T_9^{-3/2}\int_0^\infty \sigma\,E\;\exp(-11.604E/T_9)\,dE, \tag{2}$$

where A is the reduced mass in amu, and T_9 is the temperature in units of 10^9 K. The calculation of the rates is performed between $T_9 = 0.001$ and 10.

For charged-particle induced reactions, the cross section can be expressed as [FO67]

$$\sigma(E) = S(E)\;\exp(-2\pi\eta)\,\frac{1}{E}, \tag{3}$$

where $S(E)$, defined by this equation, is referred to as the astrophysical S-factor. The quantity

$$\eta = \frac{Z_1Z_2e^2}{\hbar v} = \frac{0.9895}{2\pi}\;Z_1Z_2\left(\frac{A}{E}\right)^{1/2} \tag{4}$$

is the Sommerfeld parameter, Z_1 and Z_2 being the charge numbers of the interacting nuclei, and $\hbar$ the reduced Planck constant.

2.1.2 Numerical integration of the rates

Except for narrow resonances, the S-factor is a smooth function of energy, which is convenient for extrapolating measured cross sections down to astrophysical energies. When $S(E)$ is assumed to be a constant, the integrand in Eq. (1) is peaked at the "most effective energy" [FO67]

$$E_0 = \left(\frac{\mu}{2}\right)^{1/3} \left(\frac{\pi e^2 Z_1 Z_2 k_{\rm B} T}{\hbar}\right)^{2/3} = 0.1220\ (Z_1^2 Z_2^2 A)^{1/3}\, T_9^{2/3}\ {\rm MeV} \tag{5}$$

and can be approximated by a Gaussian function centred at E_0, with full width at $1/e$ of the maximum given by

$$\Delta E_0 = 4\ (E_0\ k_{\rm B} T/3)^{1/2} = 0.2368\ (Z_1^2 Z_2^2 A)^{1/6}\, T_9^{5/6}\ {\rm MeV}. \tag{6}$$

With these approximations, the integral in Eq. (1) can be calculated analytically [FO67]. However, in the present compilation we do not rely on such approximations and perform numerically the integration of Eq. (1) for the non-resonant contribution to the rate, $N_{\rm A}\langle\sigma v\rangle_{\rm NR}$, as well as for the contribution of the broad resonances, $N_{\rm A}\langle\sigma v\rangle_{\rm BR}$. In those cases it is found that a good accuracy is reached by limiting the numerical integration for a given temperature to the energy domain $(E_0 - n\Delta E_0, E_0 + n\Delta E_0)$, with $n = 2$ or 3.

The main difficulty in evaluating the rates at the low temperatures in the range $0.001 \leq T_9 \leq 10$ is related to the necessity of extrapolating the S-factors down to very low energies, where cross sections are not available. General procedures are described in Sect. 2.2, that allow the rates to be calculated down to $T_9 = 0.001$. Their application to specific reactions is commented in Table II. Similarly, for many of the reactions considered in this compilation, $N_{\rm A}\langle\sigma v\rangle$ cannot be evaluated for temperatures as high as $T_9 = 10$ because of the lack of reliable cross section data at sufficiently high energies. In those case, we use theoretical estimates for $N_{\rm A}\langle\sigma v\rangle$ to complement the experimentally based rates up to $T_9 = 10$ according to the procedure described in Sect. 2.5.

2.1.3 Treatment of narrow resonances

In the case of a narrow resonance, the resonant cross section $\sigma_{\rm r}(E)$ is generally approximated by a Breit-Wigner expression [FO67, RO88]

$$\sigma_{\rm r}(E) \ = \ \frac{\pi}{\kappa^2}\,\omega\,\frac{\Gamma_{\rm i}(E)\ \Gamma_{\rm f}(E)}{(E - E_{\rm r})^2 + \Gamma(E)^2/4}, \tag{7}$$

where κ is the wave number, $\Gamma_{\rm i}(E)$ and $\Gamma_{\rm f}(E)$ are the entrance and exit channel partial widths, respectively, $\Gamma(E)$ is the total width, and ω is the statistical factor given by

$$\omega = (1 + \delta_{12})\frac{(2J+1)}{(2I_1+1)(2I_2+1)}, \tag{8}$$

where I_1, I_2 and J are the spins of the interacting nuclei and of the resonance. The Kronecker symbol δ_{12} takes into account that the interacting nuclei can be identical.

The energy dependence of the particle widths $\Gamma_{\rm i}(E)$ and $\Gamma_{\rm f}(E)$ is given by [LA58]

$$\Gamma_{\rm i,f}(E) = 2\gamma_{\rm i,f}^2 P_\ell(E,a) = \Gamma_{\rm i,f}\ \frac{P_\ell(E,a)}{P_\ell(E_{\rm r},a)}, \tag{9}$$

where P_ℓ is the penetration factor associated with the relative angular momentum ℓ and with the channel radius, taken as $a = 1.4\,(A_1^{1/3} + A_2^{1/3})$ fm, $\Gamma_{\rm i,f}$ are the partial widths at the resonance energy $E_{\rm r}$, and $\gamma_{\rm i,f}^2$ are the reduced widths. In absence of data, $\gamma_{\rm i,f}^2 = 0.01\gamma_{\rm W}^2$ are adopted as a first approximation, where $\gamma_{\rm W}^2 = 3\hbar^2/2\mu a^2$ is the Wigner limit.

For radiative capture reactions, the energy dependence of the gamma width $\Gamma_\gamma(E)$ is given by

$$\Gamma_\gamma(E) = \Gamma_\gamma\ \left(\frac{E - E_{\rm f}}{E_{\rm r} - E_{\rm f}}\right)^{2\lambda+1}, \tag{10}$$

where Γ_γ is the gamma width at the resonance energy E_r, λ is the multipolarity of the electromagnetic transition, and E_f is the energy of the final state in the compound nucleus.

When the Breit-Wigner cross section (7) is inserted in Eq. (1), the integrand exhibits maxima at E_r and at E_0. The contribution of the former peak corresponds to the usual resonant term $N_A\langle\sigma v\rangle_r$, while the contribution of the latter represents the so-called "tail contribution" $N_A\langle\sigma v\rangle_{tail}$. We approximate those two contributions by functions which can be integrated analytically to obtain the resonant rate as a sum of two terms:

$$\begin{aligned} N_A\langle\sigma v\rangle_R &= N_A\langle\sigma v\rangle_r + N_A\langle\sigma v\rangle_{tail} \\ &= N_A \left(\frac{2\pi}{\mu k_B}\right)^{3/2} \hbar^2\, \omega\gamma\, T^{-3/2}\, \exp(-E_r/k_BT) + N_A \left(\frac{2}{\mu}\right)^{1/2} \frac{\Delta E_0}{(k_BT)^{3/2}}\, S(E_0)\, \exp(-C_0/T^{1/3}), \end{aligned} \quad (11)$$

where $\omega\gamma$ is given by

$$\omega\gamma = \omega \frac{\Gamma_i\Gamma_f}{\Gamma(E_r)}, \quad (12)$$

and $S(E_0)$ is the S-factor calculated at energy E_0 from Eqs. (3) and (7), and

$$C_0 = 3\,(\pi^2\mu/2k_B)^{1/3}\,(e^2Z_1Z_2/\hbar)^{2/3}. \quad (13)$$

When $N_A\langle\sigma v\rangle_R$ is expressed in cm^3 mol^{-1} s^{-1}, E_r and $\omega\gamma$ in MeV, and $S(E_0)$ in MeV barn, Eq. (11) reads

$$\begin{aligned} N_A\langle\sigma v\rangle_R &= 1.5394\times10^{11}\, A^{-3/2}\, (\omega\gamma)\, T_9^{-3/2}\, \exp(-11.605E_r/T_9) \\ &\quad +7.8318\times10^{9}\, (Z_1Z_2/A)^{1/3}\, S(E_0)\, T_9^{-2/3} \exp(-4.2486(Z_1^2Z_2^2A/T_9)^{1/3}). \end{aligned} \quad (14)$$

The relative importance of these two terms depends on E_r and E_0, and hence on temperature. When $E_0 \geq E_r$, the tail contribution turns out to be negligible.

The above procedure is repeated for each narrow resonance, and their contributions to the total rate are simply added. Exceptions are made in some cases. For example, for the (α,n) reactions, the resonance data are abundant enough to allow a numerical integration of Eq. (1) in the whole energy range of interest and to avoid any of the approximations described above.

Equation (14) is also valid for the calculation of the subthreshold state contribution $N_A\langle\sigma v\rangle_{SR}$. In such cases, $\Gamma_i = 0$ ($\omega\gamma = 0$), and only the second term of Eq. (14) remains.

2.2 Data treatment

2.2.1 Resonances

When several and different data on a given resonance are published, the adopted energies E_r and strengths $\omega\gamma$ are obtained using the method of weighted average. The central value, K, and the internal and external errors, e_{int} and e_{ext}, are calculated for a set N_{exp} of data points from OV69

$$K = \frac{\sum_i W_iK_i}{\sum_i W_i}, \qquad W_i = (\Delta K_i)^{-2}, \quad (15)$$

$$e_{int} = \left(\sum_i W_i\right)^{-1/2}, \qquad e_{ext} = \left[\frac{1}{N_{exp}-1}\frac{\sum_i W_i(K_i-K)^2}{\sum_i W_i}\right]^{1/2}.$$

Here, W_i are the weighting factors, taken as ΔK_i^{-2}, where ΔK_i is the standard deviation of the data K_i. The final error is taken as $\max(e_{int}, e_{ext})$.

2.2.2 Non-resonant data

Non-resonant data points (from either one or several publications) are first expressed in terms of S-factor data points, $S(E_k) \pm \Delta S(E_k)$, where E_k is the energy corresponding to the k'th point. In general, these S-factor data are approximated by a polynomial of degree N, leading to

$$S(E) \simeq \sum_{i=0}^{N} \mathbb{S}_i E^i. \tag{16}$$

The coefficients $\mathbb{S}_i$ of this polynomial are obtained from a χ^2-fit, where the individual data points are weighted by the errors, as explained in Sect. (2.2.1). This fit is expected to be the "best" fit to different data sets, where the lower and upper limits for the $S(E)$-curve are obtained using χ^2-procedures (i.e. taking into account the ΔS_k errors). The degree N can be chosen so as to improve the quality of the fit (typical values are $N = 2$ or 3). From the S-factor (16), the reaction rates (including lower and upper limits) are calculated by numerical integration of Eq. (1) using Eq. (3).

This procedure is the standard starting point. It is easily reproducible and avoids any subjective renormalization of the different experimental data sets. However, due to the large number of different cases, this standard procedure may have to be slightly modified in specific situations (for example, renormalization might be necessary in some cases). Sometimes, a smooth spline fit to all data between the data points is adopted. These features are specified in the comments of each reaction (Table II).

For the extrapolation of the data points to zero energy, laboratory cross sections have to be corrected for electron screening (see, for example, AS87) before including them in the calculations of the rates. This effect becomes significant typically for $E/U_e \leq 100$, where U_e is the so-called screening potential, and was first observed in the ^{3}He(d,p)^{4}He reaction below 15 keV [EN88]. On the other hand, in stellar conditions, the nuclei are surrounded by a dense electron gas that reduces the Coulomb repulsion and makes penetration of the Coulomb barrier easier. The cross sections are therefore enhanced in comparison with the cross sections between bare nuclei. This stellar screening effect can be evaluated by applying, for example, the Debye-Hückel theory [CL83]. The link between stellar and laboratory conditions therefore requires the bare-nucleus cross sections. The enhancement factor due to electron screening is taken as [AS87, SC89]

$$\frac{\sigma_s(E)}{\sigma(E)} \simeq \exp(\pi\,\eta\,U_e/E) \text{ for } U_e \ll E, \tag{17}$$

where $\sigma_s(E)$ and $\sigma(E)$ are the cross sections for the screened nuclei and for the bare nuclei, respectively. The electron screening potential U_e is determined from (17) with $\sigma(E)$ extrapolated down to zero energy. A first approximation is given by $U_e = Z_1 Z_2 e^2/R_a$, where $R_a \approx a_0/Z_h$ is the atomic radius of the innermost electrons of the heaviest of the interacting atoms 1 and 2, whose charged number is denoted Z_h, a_0 being the Bohr radius.

At the present time, the Coulomb breakup method, although promising, has not been demonstrated to be a fully reliable tool. Although available measurements of this type will be quoted, they will not be taken into account in the rate evaluation. On the other hand, when experimental data do not allow the calculation of reliable reaction rates in a certain temperature range, the data are complemented with theoretical information (see, for example, Sect. 2.3).

2.2.3 Treatment of endoergic reactions

Extrapolations to low energies of endoergic reactions between charged particles are difficult as experimental data exist only at energies far above the threshold, and the existing data at the lowest energies do not allow a clear picture of the behaviour of the S-factor. This is the case for three of the reactions compiled in the present work: ^{14}N(p,α)^{11}C, ^{20}Ne(p,α)^{17}F and ^{24}Mg(p,α)^{21}Na.

The procedure for the calculation of the rates involves the S-factor of the reverse reactions S_{rev}, which smoothly depends on energy. The S-factor S_{rev} is approximated by an analytical function and extrapolated afterwards. The approximation can be a polynomial fit of the kind $S_{rev} = \sum_{i=0}^{N} \mathbb{S}_i E_\alpha^i$. This is the case of the ^{14}N(p,α)^{11}C reaction. For the ^{20}Ne(p,α)^{17}F and ^{24}Mg(p,α)^{21}Na reactions, an exponential function $S_{rev} = a_1 \exp(-a_2 E_\alpha)$ gives a better fit. The coefficients $\mathbb{S}_i$, a_1 and a_2 are obtained from a χ^2-fit. The energy E_α is the center of mass energy in the channel α+^{11}C, α+^{17}F, and α+^{21}Na, respectively.

By means of the principle of time reversal [BL52], that relates the cross section $\sigma_{12\to34}$ for the reaction $1+2\to3+4$ to the cross section $\sigma_{34\to12}$ of the reverse $3+4\to1+2$ transformation (see also Sect. 2.7), the S-factor curves and the reaction rates for the direct reactions are calculated. Details are given in the comments of the corresponding reactions.

2.3 Potential model

At low energies, the non-resonant (also called direct capture) contribution can be significant. For some of the reactions studied here at astrophysical energies, it is even the dominant process. When data required to evaluate the non-resonant part are not available, a model calculation is performed. The radiative cross section

$$\sigma(E) = \sum_{J_f,\lambda} \sigma_{J_f,\lambda}(E) \tag{18}$$

is summed over final states J_f and electric multipoles $E\lambda$. For the direct radiative capture to a state with spin J_f, the cross section for the dominant electric $E\lambda$ transition is given by

$$\sigma_{J_f,\lambda}(E) = 8\pi\alpha\frac{c}{v\kappa^2}\left[Z_1\left(\frac{A_2}{A}\right)^\lambda + Z_2\left(\frac{-A_1}{A}\right)^\lambda\right]^2 C^2S_{J_f}\sum_{J_i,I,\ell_i}\frac{(\kappa_\gamma)^{2\lambda+1}}{[(2\lambda+1)!!]^2}\frac{(\lambda+1)(2\lambda+1)}{\lambda} \tag{19}$$
$$\times\ \frac{(2\ell_i+1)(2\ell_f+1)(2J_f+1)}{(2I_1+1)(2I_2+1)}\begin{pmatrix}\ell_f & \lambda & \ell_i\\ 0 & 0 & 0\end{pmatrix}^2(2J_i+1)\begin{Bmatrix}J_i & \ell_i & I\\ \ell_f & J_f & \lambda\end{Bmatrix}^2\left(\int_0^\infty \phi_i(r)r^\lambda\phi_f(r)\,dr\right)^2,$$

where κ_γ is the photon wave number, ℓ_i and ℓ_f are the initial and final orbital angular momenta, I is the channel spin, $\begin{pmatrix}\ell_f & \lambda & \ell_i\\ 0 & 0 & 0\end{pmatrix}$ and $\begin{Bmatrix}J_i & \ell_i & I\\ \ell_f & J_f & \lambda\end{Bmatrix}$ are the $3j$ and $6j$ symbols, and ϕ_i and ϕ_f are the initial and final wave functions, solutions of the radial Schrödinger equation

$$\left[-\frac{\hbar^2}{2\mu}\left(\frac{d^2}{dr^2}-\frac{\ell(\ell+1)}{r^2}\right)+V^{J\ell I}(r)\right]\phi(r) = E\,\phi(r), \tag{20}$$

where the potential $V^{J\ell I}(r)$ is adjusted so as to reproduce the energies of the final bound states. It has been shown in BA85 that adjusting the potential to the final bound state gives a good estimate. This equation is solved numerically. In Eq. 20, $C^2S_{J_f}$ is the spectroscopic factor of the final state, assumed to be $C^2S_{J_f}=1$ for the reactions considered here. The initial scattering wave function is normalized asymptotically as

$$\phi_i \underset{r\to\infty}{\to} \cos\delta^{J_i\ell_iI}F_{\ell_i}(\kappa r) + \sin\delta^{J_i\ell_iI}G_{\ell_i}(\kappa r), \tag{21}$$

where F_ℓ and G_ℓ are the regular and irregular Coulomb wave functions, and $\delta^{J\ell I}$ is the phase shift. The channel spin I is equal to the total spin of the final state. The orbital momentum of the initial state is chosen as the smallest value compatible with the orbital momentum ℓ_f of the bound state and the multipolarity λ.

2.4 Analytical approximation of reaction rates

The major goal of the present compilation is to provide numerical reaction rates in tabular form. This approach differs from the one promoted in previous compilations (CA88 and references therein), and is expected to lead to more accurate rates. However, for completeness, we also provide analytical approximations to the numerical adopted rates. For this purpose, the total rate is expressed as

$$N_{\rm A}\langle\sigma v\rangle = N_{\rm A}\langle\sigma v\rangle_{\rm NR+tail} + N_{\rm A}\langle\sigma v\rangle_{\rm r} + N_{\rm A}\langle\sigma v\rangle_{\rm MR} + N_{\rm A}\langle\sigma v\rangle_{\rm SR} + N_{\rm A}\langle\sigma v\rangle_{\rm BR}, \tag{22}$$

where the various contributions are discussed in Sects. 2.4.1–2.4.5 below.

2.4.1 Non-resonant and tail contribution to the rates

The non-resonant rate, $N_{\rm A}\langle\sigma v\rangle_{\rm NR}$ (Sect. 2.1.2), and the tail contribution to the rate, $N_{\rm A}\langle\sigma v\rangle_{\rm tail}$ (second term in the r. h. s. of Eq. (14)), are approximated by the same formula, and are lumped in a single contribution $N_{\rm A}\langle\sigma v\rangle_{\rm NR+tail}$. For an exoergic reaction, with Q-value Q, it takes the form

$$N_{\rm A}\langle\sigma v\rangle_{\rm NR+tail} = C_1 T_9^{-2/3} \exp(-C_0\, T_9^{-1/3}) \left(1 + \sum_{i=1}^{N_{\rm rate}} c_i T_9^i\right) \qquad [Q > 0]. \tag{23}$$

The coefficients C_1 and c_i are fitted to the rate contributions calculated as described in Sects. 2.1.2 and 2.1.3, and $C_0 = 4.2486(Z_1^2 Z_2^2 A)^{1/3}$ (from Eq. (13)). The degree $N_{\rm rate}$ of the polynomial in Eq. (23) is chosen in order to obtain fits accurate to a few percent, and typically better than 10%–15%. Equation (23) is found to provide a better approximation than the $T_9^{1/3}$ expansion adopted in previous compilations (Eq. (50) in FO67).

For endoergic reactions, $N_{\rm A}\langle\sigma v\rangle_{\rm NR+tail}$ is parametrized as [BA69a]

$$N_{\rm A}\langle\sigma v\rangle_{\rm NR+tail} = C_1 T_9^{-2/3} \exp(-C_0'\, T_9^{-1/3} - D_0/T_9) \left(1 + \sum_{i=1}^{N_{\rm rate}} c_i T_9^i\right) \qquad [Q < 0], \tag{24}$$

where

$$D_0 = \mid Q \mid /k_{\rm B} = 11.605 \mid Q \mid, \tag{25}$$

Q being expressed in MeV and C_1 and c_i are adjustable parameters. The coefficient $C_0^{'}$ is computed from Eq. (13) with the nuclear charges and masses corresponding to the exit channel.

2.4.2 Isolated and narrow resonance rates

The contribution of isolated and narrow resonances is given by the first term of Eq. (14),

$$N_{\rm A}\langle\sigma v\rangle_{\rm r} \;=\; D_1 T_9^{-3/2} \exp(-D_2/T_9), \tag{26}$$

with

$$D_1 = N_{\rm A} \left(\frac{2\pi}{\mu k_{\rm B}}\right)^{3/2} \hbar^2(\omega\gamma) = 1.5394 \times 10^{11} A^{-3/2}\, \omega\gamma, \tag{27}$$

and

$$D_2 = E_{\rm r}/k_{\rm B} = 11.605\ E_{\rm r}. \tag{28}$$

The analytical approximations include the isolated and narrow resonances with the most significant contribution.

2.4.3 Multiresonant rates

For high densities of resonances (energy spacings of the order of the resonance widths, or even overlapping resonances), it is found that a continuum background is superimposed on some sharp resonances. While these narrow resonances can be accounted for by Eqs. (26)-(28), it is advisable to represent the continuum by one multiresonance (MR) term of the form

$$N_{\rm A}\langle\sigma v\rangle_{\rm MR} = D_3\ T_9^{D_4}\ \exp(-D_5/T_9). \tag{29}$$

The parameters D_3, D_4 and D_5 are obtained from a fit to the numerical values of the rates.

2.4.4 Subthreshold states

When a subthreshold state is present, its contribution $N_{\rm A}\langle\sigma v\rangle_{\rm SR}$ to the rate is obtained through a modification of Eq. (23) which reads

$$N_{\rm A}\langle\sigma v\rangle_{\rm SR} \;=\; C_1 T_9^{-2/3}\, S(E_0)\, \exp(-C_0\, T_9^{-1/3}) \left(1 + \sum_{i=1}^{N_{\rm rate}} c_i T_9^i\right), \tag{30}$$

where C_1 and c_i are adjustable parameters. Using Eqs. (3) and (7), the S-factor is found to depend on energy as

$$S(E) = S_{\rm r}\,\frac{1}{(E-E_{\rm r})^2+\Gamma^2/4}, \tag{31}$$

where $S_{\rm r} = S(E_{\rm r})$. Taking into account that $E_{\rm r} < 0$ and that Γ is very small, the energy dependence of the S-factor can be approximated by $1/E^2$. With this result, Eq. (30) is rewritten as

$$N_{\rm A}\langle\sigma v\rangle_{\rm SR} \;=\; C_1 T_9^{-2}\exp(-C_0\,T_9^{-1/3})\left(1+\sum_{i=1}^{N_{\rm rate}} c_i T_9^i\right), \tag{32}$$

where C_1 and c_i are adjustable parameters.

2.4.5 Broad low energy resonances

When a broad low energy resonance ($\Gamma > E_{\rm r}$) is present, the S-factor is not well approximated by a polynomial. In contrast to the case of subthreshold states, the denominator of Eq. (31) cannot be approximated by E^2. The contribution to the total reaction rate of a broad low energy resonance can be written as

$$N_{\rm A}\langle\sigma v\rangle_{\rm BR} \;=\; C_1 T_9^{-2/3}\exp(-C_0\,T_9^{-1/3})\,\frac{1}{[E_0(T_9)-E_{\rm r}]^2+\Gamma^2/4}\left(1+\sum_{i=1}^{N_{\rm rate}} c_i T_9^i\right), \tag{33}$$

where C_1 and c_i are adjustable parameters.

2.5 Hauser-Feshbach rates

When cross section data do not allow the calculation of $N_{\rm A}\langle\sigma v\rangle$ up to $T_9 = 10$, we use theoretical predictions obtained with the Hauser-Feshbach model in a range $T_{9,\max} < T_9 \leq 10$, where $T_{9,\max}$ is defined as follows. Let us denote $E_{\max}$ as the highest centre-of-mass energy for which a cross section measurement is available. A reliable calculation of $N_{\rm A}\langle\sigma v\rangle$ on the basis of the available measurements can be done at a given temperature if the contribution of the integrand of Eq. (2) for $E > E_{\max}$ can be neglected at that temperature. This requirement is examined for each considered reaction, and is found to be satisfied if one takes $E_0 + n\Delta E_0 = E_{\max}$ with $n = 1$ to 3, depending on the reaction. From this condition, $T_{9,\max}$ is deduced with the help of Eqs. (5) and (6). Note that, in a few instances (specified in the comments of Table II), it is considered that the mere use of a constant S-factor up to the energy $E_0 + n\Delta E_0$ corresponding to $T_9 = 10$ is sufficient, not leading to a significant loss of accuracy, so that the use of Hauser-Feshbach rates is not necessary.

In short, the Hauser-Feshbach (HF) calculations proceed as follows. Let us consider the reaction $1^\alpha + 2 \rightarrow 3^\beta + 4$, where α and β represent bound states in target nucleus 1 and residual nucleus 3 with excitation energies ϵ_1^α and ϵ_3^β and with spins I_1^α and I_3^β, respectively (the ground states of 1 and 3 correspond to $\alpha = 0$ and $\beta = 0$). We consider reactions where particles 2 and 4, with spins I_2 and I_4, are neutrons, protons, α-particles or photons and have no bound excited states. The HF theory assumes that the reaction proceeds through the formation of a compound nucleus and that the cross section is given by

$$\sigma_{\alpha\beta}(E^\alpha) \;=\; \frac{\pi\hbar^2/2\mu E^\alpha}{(2I_1^\alpha+1)(2I_2+1)}\sum_{J,\pi}(2J+1)\frac{T^\alpha(J^\pi)T^\beta(J^\pi)}{T_{\rm tot}(J^\pi)}W_{\alpha\beta}, \tag{34}$$

where 1^α and 2 interact with centre-of-mass energy $E^\alpha = E - \epsilon_1^\alpha$. The quantities $T^\alpha(J^\pi)$ and $T^\beta(J^\pi)$ are the transmission functions for forming the state J^π in the compound nucleus from $1^\alpha + 2$ and $3^\beta + 4$, respectively. The statistical model assumes that such a state exists for each orbital angular momentum of the relative motion between 1 and 2 at the corresponding excitation energy of the compound nucleus. Each T is a summation over all possible orbital and channel spins. The total transmission function $T_{\rm tot}(J^\pi)$ is the sum of all the transmission functions for the decay of the compound state J^π into any possible (bound or unbound) state energetically accessible from $1^\alpha + 2$ interacting with energy E^α, while $W_{\alpha\beta}$ is the width fluctuation correction factor.

The total cross section $\sigma_\alpha(E^\alpha)$ for the reaction $1^\alpha + 2 \rightarrow 3 + 4$ to all bound states of the residual nucleus is obtained by summing over β both sides of Eq. (34), and the laboratory measurements provide the cross section $\sigma_0(E)$ on the target ground state. When the residual nucleus has an isomeric state, it may be of interest to distinguish the reaction leading to that state from the reaction producing the residual nucleus in its ground state. Such a distinction cannot be made in our HF calculations. The particular treatment of the reactions $^{25}\mathrm{Mg(p,\gamma)}^{26}\mathrm{Al}^{g,m}$ is described in the comments of Table II.

We briefly describe here the nuclear physics ingredients used in our HF calculations. The γ-transmission functions include the dominant E1 and M1 transitions only. The transmission functions for neutrons and protons are calculated using optical potentials derived by JE77, while the phenomenological Woods-Saxon potential of MA78a is used for the calculation of α-particle transmission functions. We refer to TH86 for further references and details concerning the calculation of transmission functions. The summation over nuclear excited states which appears in Eq. (34) transforms into an integral over a nuclear level density as soon as the channel energy exceeds the energy of the last excited level for which energy, spin and parity are known experimentally. The experimental nuclear levels are taken from the Nuclear Data Sheets up to 1995, and a level density formula based on the back-shifted Fermi gas formalism with empirical shell corrections [TH86] is adopted. The nuclear masses are from AU97. The use of a statistical reaction theory may seem inappropriate in the case of very light nuclei. However, we observe that, for the 27 reactions requiring HF calculations, the rates derived from experiments differ from the theoretical ones at $T_9 = T_{9,\mathrm{max}}$ by less than a factor 7, except in 2 cases, where they differ by factors 14 and 34.

In order to keep a reasonable balance between the reliability of our experimentally-based rates and the relatively good quality of the HF predictions (being expected to be better at higher than at lower temperatures), we adopt the following procedure in the $T_{9,\mathrm{max}} < T_9 \leq 10$ range. Let us denote $\langle \sigma v \rangle_a$, $\langle \sigma v \rangle_h$ and $\langle \sigma v \rangle_l$ the recommended rates and their estimated upper and lower limits, where the indices a, h and l stand for *adopt*, *high* and *low* as in Table II (see Sect. 3). Upper indices "max" and "10" refer to the values of those quantities at $T_9 = T_{9,\mathrm{max}}$ and at $T_9 = 10$, respectively. A typical situation is shown in Fig. 1 for the case where the calculated HF rate is larger than the adopted one at $T_{9,\mathrm{max}}$ (Fig.1, upper panel).

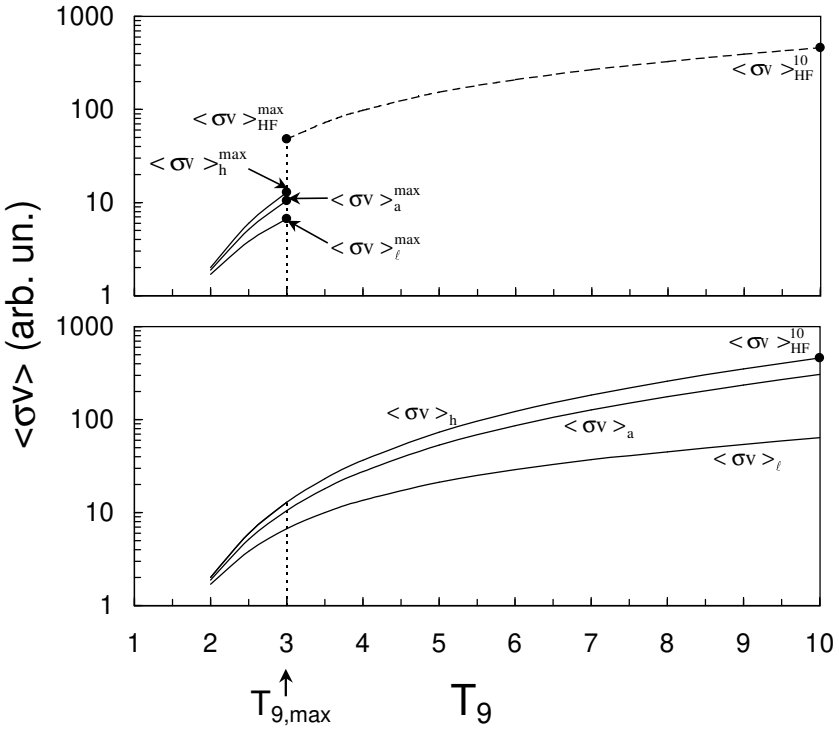

Figure 1: Construction of the adopted rate and of its upper and lower limits in the range $T_{9,\mathrm{max}} < T_9 \leq 10$. Upper panel: the evaluated rates $\langle \sigma v \rangle_a$, $\langle \sigma v \rangle_l$ and $\langle \sigma v \rangle_h$ for $T_9 \leq T_{9,\mathrm{max}}$ and the HF estimate for $T_{9,\mathrm{max}} < T_9 \leq 10$; lower panel: $\langle \sigma v \rangle_a$, $\langle \sigma v \rangle_l$ and $\langle \sigma v \rangle_h$ calculated up to $T_9 = 10$ by the procedure outlined in the text.

In such a case,
1) $\langle \sigma v \rangle_l$ is assumed to vary like the HF rate $\langle \sigma v \rangle_{\rm HF}$. Having to be continuous at $T_{9,\rm max}$, it is simply given by

$$\langle \sigma v \rangle_l = \langle \sigma v \rangle_{\rm HF} \frac{\langle \sigma v \rangle_l^{\rm max}}{\langle \sigma v \rangle_{\rm HF}^{\rm max}}; \tag{35}$$

2) we consider that the upper limit of the rate at $T_9 = 10$ is given by $\langle \sigma v \rangle_{\rm HF}^{10}$. To connect $\langle \sigma v \rangle_h^{\rm max}$ to $\langle \sigma v \rangle_h^{10}$ we multiply $\langle \sigma v \rangle_{\rm HF}$ according to

$$\langle \sigma v \rangle_h = \langle \sigma v \rangle_{\rm HF} \left(\frac{10 - T_9}{10 - T_{9,\rm max}} \frac{\langle \sigma v \rangle_h^{\rm max}}{\langle \sigma v \rangle_{\rm HF}^{\rm max}} + \frac{T_9 - T_{9,\rm max}}{10 - T_{9,\rm max}} \right) \tag{36}$$

where the multiplicative factor varies linearly with T_9 and has the correct values at $T_{9,\rm max}$ and 10;
3) $\langle \sigma v \rangle_a$ is obtained by requiring that the ratio of the errors made on $\langle \sigma v \rangle$ remains constant in the $T_{9,\rm max} < T_9 \leq 10$ range,

$$\frac{\langle \sigma v \rangle_h - \langle \sigma v \rangle_a}{\langle \sigma v \rangle_a - \langle \sigma v \rangle_l} = \frac{\langle \sigma v \rangle_h^{\rm max} - \langle \sigma v \rangle_a^{\rm max}}{\langle \sigma v \rangle_a^{\rm max} - \langle \sigma v \rangle_l^{\rm max}}. \tag{37}$$

Similar prescriptions are used for the determination of $\langle \sigma v \rangle_a$, $\langle \sigma v \rangle_h$ and $\langle \sigma v \rangle_l$ when $\langle \sigma v \rangle_{\rm HF}^{\rm max} < \langle \sigma v \rangle_a^{\rm max}$, the treatment of $\langle \sigma v \rangle_l$ and $\langle \sigma v \rangle_h$ being interchanged in this case.

2.6 Effect of the thermal excitation of target nuclei

In a stellar plasma, the excited levels of a target nucleus are thermally populated, and thus contribute to the reaction mechanism. As a result, the stellar rates may differ from those obtained when the target nuclei are in their ground state. This correction cannot be predicted on grounds of experimental data, except in very specific situations (see e. g. BA69b). These are considered in CA88 (Table II) through appropriate corrections in their analytical expressions, whenever those authors consider it to be important. In the other instances, they evaluate the thermalization effects with the use of the so-called "equal strength approximation". In this rough approach, the rate on a thermalized target is just identical to the ground state rate (see FO75, p. 90, for a thorough discussion of the CA88 procedure). Here, we evaluate this effect in the framework of the HF model by calculating the population of the target excited states under the assumption that the stellar plasma is in local thermodynamic equilibrium (LTE). In this case the relative population of the various states is simply Maxwellian. The ratio of the HF rates on a thermalized target to the HF rates for a target in its ground state is then given by

$$r_{\rm tt} = \frac{1}{G_1(T)} \sum_\alpha \frac{(2J_1^\alpha + 1)}{(2J_1^0 + 1)} \exp\left(-\frac{\epsilon_1^\alpha}{kT}\right) \frac{\langle \sigma_\alpha v \rangle_{\rm HF}}{\langle \sigma_0 v \rangle_{\rm HF}} \tag{38}$$

where

$$G_i(T) = \frac{1}{2J_i^0 + 1} \sum_\mu (2J_i^\mu + 1) \exp\left(-\frac{\epsilon_i^\mu}{kT}\right) \tag{39}$$

is the temperature-dependent, normalized partition function for nucleus i. The temperature-dependent partition functions (39) are given in Table IV in the form of analytical expressions in T_9 for all concerned target and residual nuclei.

The use of the HF theory to calculate r_{tt} is justified by the previous discussion on the validity of HF for describing the ground state rate $\langle \sigma_0 v \rangle$ since the reaction from a target excited level shifts the energy of the compoud nucleus by the energy of that level, so that the number of available compound nucleus levels is increased. On the other hand, in all considered cases, the temperature dependence of the rates is very smooth at temperatures where thermal effects are expected to be important. As a result, very large variations of $\langle \sigma_\alpha v \rangle$ due to the presence of isolated resonances, which would be overlooked by using a statistical description of the involved nuclear spectra, are very improbable. Although one cannot exclude that the use of the HF model can accidentally introduce errors in r_{tt}, we consider that most of the

uncertainty is removed by expressing r_{tt} as a ratio of two HF estimates.

For each reaction, the values of $N_{\rm A}\langle\sigma v\rangle_{\rm gs}$ given in the tables (see Sect. 3) have to be multiplied by $r_{\rm tt}$ in order to obtain the "thermalized" rates $N_{\rm A}\langle\sigma v\rangle_{\rm tt}$ which are of direct astrophysical relevance. The same correction applies to the *low*, *adopted* and *high* rates. For nuclei with $Z > 5$, and when $r_{\rm tt}$ differs from unity by more than 3% at one temperature at least of the considered range ($r_{\rm tt}$ can be either > 1 or < 1), $r_{\rm tt}$ is approximated by analytical formulae which are given in Table III. In the other cases, we just adopt $N_{\rm A}\langle\sigma v\rangle_{\rm tt} = N_{\rm A}\langle\sigma v\rangle_{\rm gs}$. The errors made by using the formulae of Table III are in general negligible, and can reach 5% only for large corrections (in excess of 50%).

Note that if the target nucleus has an isomeric state, its population relative to the others states is not always Maxwellian in the considered temperature range, and the above prescription has to be modified. We refer to the comments of Table II for the particular case of the reaction ^{26}Al(p,γ)^{27}Si.

The thermalization corrections are most pronounced when low lying excited states of the target nuclei can be strongly populated in the considered temperature range, and when the probability of an outgoing channel is strongly dependent on momentum-parity selection rules. This is particularly true for endoergic reactions which have particle channels as final states (see e.g. AR72). The corrections exceed 50% at some temperatures in the considered temperature range for 11 reactions: 7 of those are endoergic (p,n), (p,α) or (α,n) reactions, for which the corrections reach a factor 2 or more. Note that several large corrections are obtained for temperatures smaller than $T_9 = 10$, which shows the role played by the momentum-parity selection rules on the thermalization effect.

2.7 Reverse reaction rates

The principle of time-reversal invariance [BL52] relates the cross section $\sigma_{12\rightarrow 34}$ for the reaction $1+2 \rightarrow 3+4$ to the cross section $\sigma_{34\rightarrow 12}$ of the reverse $3+4 \rightarrow 1+2$ transformation. On these grounds, and provided that the rates for the direct and for the inverse reactions are thermalized, their ratio is given by

$$\frac{\langle\sigma v\rangle_{34\rightarrow 12}}{\langle\sigma v\rangle_{12\rightarrow 34}} = \frac{(2I_1+1)(2I_2+1)(1+\delta_{34})}{(2I_3+1)(2I_4+1)(1+\delta_{12})} \left(\frac{G_1G_2}{G_3G_4}\right) \left(\frac{A_1A_2}{A_3A_4}\right)^{3/2} \exp\left(-\frac{Q}{k_{\rm B}T}\right), \quad (40)$$

where Q is the Q-value for reaction $1+2 \rightarrow 3+4$ and G_i are the temperature-dependent partition functions for nuclei $i = 1$ to 4, defined by Eq. (39). Note than $G_i(T) \equiv 1$ for nucleons and for nuclei which have no bound excited states.

The summation on the excited states μ of the nucleus i is performed as in the case of Eq. (34) (see Sect. 2.5). When "particle" 4 is a photon, the photodisintegration rate (in s^{-1}) for the reaction $3+\gamma \rightarrow 1+2$ is written as

$$\lambda_{3\gamma\rightarrow 12} = \frac{(2I_1+1)(2I_2+1)}{(2I_3+1)(1+\delta_{12})} \left(\frac{G_1G_2}{G_3}\right) \left(\frac{A_1A_2}{A_3}\right)^{3/2} \left(\frac{k_{\rm B}T}{2\pi N_A\hbar^2}\right)^{3/2} \langle\sigma v\rangle_{12\rightarrow 3\gamma} \exp\left(-\frac{Q}{k_{\rm B}T}\right) \quad (41)$$

$$= 9.8686\times 10^9 T_9^{3/2} \frac{(2I_1+1)(2I_2+1)}{(2I_3+1)(1+\delta_{12})} \left(\frac{G_1G_2}{G_3}\right) \left(\frac{A_1A_2}{A_3}\right)^{3/2} N_{\rm A}\langle\sigma v\rangle_{12\rightarrow 3\gamma} \exp\left(-11.605\, Q/T_9\right). \quad (42)$$

A few of the compiled reactions involve 3 particles in the outgoing channel. Although the expression of $N_{\rm A}\langle\sigma v\rangle$ for the direct reaction $1+2 \rightarrow 3+4+5$ is still given by Eq. (1), the reverse/direct rate ratio is given by:

$$\frac{\langle\sigma v\rangle_{345\rightarrow 12}}{\langle\sigma v\rangle_{12\rightarrow 345}} = \frac{(2I_1+1)(2I_2+1)\, n_{345}!}{(2I_3+1)(2I_4+1)(2I_5+1)(1+\delta_{12})} \left(\frac{G_1G_2}{G_3G_4G_5}\right) \left(\frac{A_1A_2}{A_3A_4A_5}\right)^{3/2} \left(\frac{2\pi N_{\rm A}\hbar^2}{k_{\rm B}T}\right) \exp\left(-\frac{Q}{k_{\rm B}T}\right) \quad (43)$$

where n_{345} is the number of identical particles among 3, 4 and 5.

In Table III, we give the reverse ratio for each reaction ("Rev. ratio") *without* the partition functions $G_i(T)$. The complete reverse ratio is obtained by using the partition functions of Table IV. The special cases of the two 3-body reactions are treated in comments of Table II.

3 PRESENTATION OF RESULTS

The compilation is concerned only with reaction rates that are large enough for the target lifetime to be shorter than the age of the Universe, taken to be equal to 15×10^9 y. Assuming a density of 10^4 g cm^{-3}, reactions rates with values

$$N_{\rm A}\langle\sigma v\rangle \leq 10^{-25} \text{ cm}^3 \text{ mol}^{-1} \text{ s}^{-1}$$

can be considered as negligible in practically all astrophysical conditions. If $N_{\rm A}\langle\sigma v\rangle$ is always larger than 10^{-25} cm^3 mol^{-1} s^{-1}, the lowest temperature T_9 is taken as 0.001, as in previous compilations. Larger densities can be met in various astrophysical phenomena, but only on a much shorter time scale.

Table I lists the compiled reactions. Reaction rates are given in Table II. For each reaction, some comments concerning the adopted experimental data are given, along with the way the calculation of the rates has been performed. If necessary, a table of narrow resonances is given. It contains the energies $E_{\rm r}$ and strengths $\omega\gamma$ of an ensemble of relatively low energy resonances of relevance. For each of them, the source references are provided. In a variety of cases, more resonances than the explicitly tabulated ones are included in the rate calculation. Their taking into account is reminded in the resonance table, and the corresponding list of original references is given in the comments. A weighted average of the available resonance strengths is adopted for the calculation of the rates, except otherwise stated. For resonances where only an upper limit of the strength is reported, the adopted value is obtained by multiplying the upper limit by 0.1. The "error" on the adopted value corresponds to applying a factor 0 and 1 to obtain the lower and upper limits, respectively. The last column of the table shows whether the resonance has been treated as an isolated term (I), or included in a multiresonance term (M) in the analytical approximation. If its contribution is negligible (N), it is not included in the analytical approximation.

Figures of the S-factor versus energy are also given, where applicable. They show all published data sets, even those that are not adopted for the calculation of the rates. A temperature scale is also given. It is obtained by inverting Eq. (5), which gives the "most effective energy" E_0 as a function of temperatures. The solid curves correspond either to the adopted S-factor in the whole energy range covered by experiments, or to an extrapolation to lower energies. In the first case, the adopted curve is, in most cases, a polynomial fit. However, in some reactions, the adopted rate is calculated using the energy dependence given by theoretical calculations. Details about the adopted procedure are found in the comments. If only an extrapolation curve is shown, the rates are calculated using a spline curve though the experimental data and extrapolated to zero energy by the displayed curve. The Q-value is also shown for endoergic reactions.

The calculation of the reaction rates is performed as explained in Sect.2. The results are presented in a tabular way in Table II as a function of T_9. The temperature steps are the same as in CA88. The columns labeled *low, adopt, high* display the lower limit, adopted value, and upper limit of $N_{\rm A}\langle\sigma v\rangle_{\rm gs}$. The column labeled *exp* is the exponent n of the factor 10^n that should multiply the three previous columns. Our adopted $N_{\rm A}\langle\sigma v\rangle_{\rm tt}$ rates can be calculated as the product of the entries of column *adopt* by the values of $r_{\rm tt}$, an analytical approximation of which is given in Table III. The column *ratio* displays the ratios between these adopted $N_{\rm A}\langle\sigma v\rangle_{\rm tt}$ and the *intermediate* rates proposed by CA88. This ratio may thus be affected by the respective predictions of both the ground state rate and the thermalized rate. Cases where our $r_{\rm tt}$ HF predictions differ from the CA88 equal strength approximation ($r_{\rm tt} = 1$) by more than 10% are duly identified in the specific comments to the rates.

Analytical approximations for the adopted reaction rates $N_{\rm A}\langle\sigma v\rangle_{\rm gs}$ and $N_{\rm A}\langle\sigma v\rangle_{\rm tt}$ are given in Table III, along with an analytical approximation of the factor (Rev. ratio) by which $N_{\rm A}\langle\sigma v\rangle_{\rm tt}$ has to be multiplied in order to derive the reverse rate on the corresponding thermalized nucleus.

Acknowledgments

We express our appreciation to G. Audi for his useful advice. We are grateful to S. Goriely, N. Grama, J. Kiener, G. Meynet, N. Prantzos, and J.P. Thibaud for interesting discussions. We thank L. Buchmann, B. W. Filippone, R.W. Kavanagh, S. Kubono, J.D. King, and V. McLane for some useful data and information. We also thank L. Brito, M. Coraddu, A. D'Alessandro, U. Greife, L. Heyvaert-Biron, M. Jaeger, M. Junker, G. Mezzorani, J. Nickel, F. de Oliveira, C. Plettner, A. Schiller, F. Strieder, and O. Wieland for their assistance during this work. This work was supported by the European Commission under the Human Capital and Mobility network contract ERBCHRXCT930339 and the PECO-NIS contract ERBCIPDCT940629.

Appendix A: Notations

Throughout this work, we use the following symbols and conventions. When symbols of physical quantities must be replaced by numerical values, the units given in brackets are used implicitly (unless otherwise stated) throughout this paper.

α	=	fine structure constant
γ^2	=	reduced resonance width
Γ, $\Gamma(E)$	=	total width in the centre-of-mass system (MeV)
$\Gamma_{\rm i}(E)$, $\Gamma_{\rm f}(E)$	=	partial widths of the entrance and exit channels in the centre-of-mass system (MeV)
δ_{ij}	=	Kronecker symbol
η	=	Sommerfeld parameter
κ	=	particle wave number
κ_γ	=	photon wave number
λ	=	order of the electric multipole moment
μ	=	reduced mass
σ, $\sigma(E)$	=	cross section (barn)
$\sigma_{\rm r}$	=	resonant cross section (barn)
ϕ_i, ϕ_f	=	initial and final radial wave functions
$\omega\gamma$	=	resonance strength in the centre-of-mass system (MeV)
a_0	=	first Bohr radius
A_i	=	mass of nucleus i (amu)
A	=	reduced mass (amu). For a two-body system $1+2$, $A = A_1A_2/(A_1+A_2)$ (amu)
c	=	light velocity
e	=	proton charge
E	=	energy in the centre-of-mass system (MeV)
E_γ	=	energy of the emitted gamma ray (MeV)
$E_{\rm i,f}$	=	energy of the initial, final state in the compound nucleus (MeV)
$E_{\rm r}$	=	resonant energy in the centre-of-mass system (MeV)
E_0	=	most effective energy (MeV)
$E_{\rm x}$	=	excitation energy with respect to the ground state (MeV)
ΔE_0	=	full $1/e$ width of the Gamow window (MeV)
F_ℓ, G_ℓ	=	regular, irregular Coulomb wave function
$\hbar$	=	reduced Planck constant
I_i	=	spin of the interacting nucleus i in units of $\hbar$
I	=	channel spin in units of $\hbar$, $I = I_1 \otimes I_2$
J	=	resonance spin in units of $\hbar$
J_f	=	spin of a compound state in units of $\hbar$
$k_{\rm B}$	=	Boltzmann constant
ℓ	=	relative orbital angular momentum in units of $\hbar$
ℓ_i, ℓ_f	=	initial, final orbital angular momentum in units of $\hbar$
$N_{\rm A}$	=	Avogadro number
$N_{\rm A}\langle\sigma v\rangle$	=	reaction rate (cm^3 mol^{-1} s^{-1})
$N_{\rm A}\langle\sigma v\rangle_{\rm gs}$	=	reaction rate for the target nucleus in ground state (cm^3 mol^{-1} s^{-1})
$N_{\rm A}\langle\sigma v\rangle_{\rm ms}$	=	reaction rate for the target nucleus in isomeric state (cm^3 mol^{-1} s^{-1})
$N_{\rm A}\langle\sigma v\rangle_{\rm tt}$	=	reaction rate for a thermalized target nucleus (cm^3 mol^{-1} s^{-1})
Q	=	reaction Q-value (MeV)
r	=	radial variable describing the relative motion of particles
$R_{\rm a}$	=	atomic radius
$S(E)$	=	astrophysical S-factor (MeV barn)
$S_{\rm r}$	=	S-factor at the resonance energy $E_{\rm r}$ (MeV barn)
T	=	temperature
T_9	=	temperature in 10^9 K
v	=	relative velocity
Z_i	=	charge number of interacting nucleus i

Appendix B: Physical constants and atomic masses

The following physical and conversion constants are used in all calculations related to the present compilation. They are taken from the 1996 report of the Particle Data Group [PA96] and, with the exception of c, are rounded to a maximum of 6 significant digits. For atomic masses, the central values of the AU97 compilation are used, rounded to the microamu level.

Although the physics involved in the cross section and reaction rate evaluation most often does not require the level of accuracy used for the atomic masses and for the following constants, any detailed comparison the reader wishes to make between his/her reaction rates and ours should use the same values in order to avoid artificial numerical discrepancies.

Note that, at the present level of accuracy, the last significant digit of our constants is neither affected by the 1-standard deviation uncertainties quoted in [PA96] (the quoted value of c is exact by definition, being used to define the meter), nor by the new recommended value for the constant $(2e/h)$ used in [AU97].

$$
\begin{array}{lcl}
c & = & 299792458 \text{ m s}^{-1} \\
1 \text{ amu} & = & 931.494 \text{ MeV}/c^2 \\
1 \text{ eV} & = & 1.60218 \times 10^{-19} \text{ J} \\
k_{\rm B}T & = & 0.08617\, T_9 = T_9/11.605 \text{ MeV} \\
N_{\rm A} & = & 6.0221 \times 10^{23} \text{ mol}^{-1} \\
\alpha & = & e^2/\hbar c = 1/137.036 \\
\hbar c & = & 197.327 \text{ MeV fm}
\end{array}
$$

EXPLANATION OF TABLES

Table I. Summary of compiled reactions

Reaction	the reaction in conventional notation
Notation in refs.	notation used in references for each reaction

Table II. Reaction Rates

Reaction		the reaction in conventional notation
Comments		specific comments on the compilation procedure
S-factor figure		presentation of S-factor versus c.m. energy
Resonance table		tabular presentation of resonance properties
	E_r	resonance energy in c.m. system (in keV or MeV)
	J^π	resonance spin and parity
	$\omega\gamma$	resonance strength in c.m. system (in meV, eV or keV)
	adopt	adopted resonance strength in c.m. system
Table of rates		tabular presentation of rates
	T_9	temperature in units of 10^9 K
	lower	lower limit of the rates
	adopt	recommended rates
	upper	upper limit of the rates
	exp	exponent n of the factor 10^n that should multiply the three previous columns
	ratio	ratio of the adopted rate $N_A\langle\sigma v\rangle_{tt}$ to the CA88 rate

Table III. Analytical approximation of the reaction rates

Reaction	the reaction in conventional notation
Q	Q-value of the reaction in MeV
(n%)	accuracy of the analytical approximation with respect to the tabulated rates, "better than n%"
gs, ms, tt	indicate reactions with target nuclei in ground state, isomeric state, or with thermalized target
g, m, t	indicate reactions leading to the ground state, isomeric state, or to both ground and isomeric states
Rev. ratio	factor by which the rate $N_A\langle\sigma v\rangle_{tt}$ has to be multiplied in order to get the rate of the reverse reaction on the corresponding thermalized nucleus

Table IV. Analytical approximation of the partition functions

$G(T_9)$	partition function
isotope	isotope in conventional notation
a_1, a_2, a_3, a_4, a_5	coefficients of the analytical approximation

The accuracy of the analytical approximations is better than 2%

Table I. List of compiled reactions

Reaction	Notation in refs.	Reaction	Notation in refs.	Reaction	Notation in refs.
^{1}H(p,νe^{+})^{2}H	ppnu	^{11}B(p,α)^{8}Be	b11pa	^{20}Ne(p,α)^{17}F	ne20pa
^{2}H(p,γ)^{3}He	dpg	^{12}C(p,γ)^{13}N	c12pg	^{20}Ne(α,γ)^{24}Mg	ne20ag
^{2}H(d,γ)^{4}He	ddg	^{12}C(α,γ)^{16}O	c12ag	^{21}Ne(p,γ)^{22}Na	ne21pg
^{2}H(d,n)^{3}He	ddn	^{13}C(p,γ)^{14}N	c13pg	^{21}Ne(α,n)^{24}Mg	ne21an
^{2}H(d,p)^{3}H	ddp	^{13}C(p,n)^{13}N	c13pn	^{22}Ne(p,γ)^{23}Na	ne22pg
^{2}H(α,γ)^{6}Li	dag	^{13}C(α,n)^{16}O	c13an	^{22}Ne(α,γ)^{26}Mg	ne22ag
^{3}H(d,n)^{4}He	tdn	^{13}N(p,γ)^{14}O	n13pg	^{22}Ne(α,n)^{25}Mg	ne22an
^{3}H(α,γ)^{7}Li	tag	^{14}N(p,γ)^{15}O	n14pg	^{22}Na(p,γ)^{23}Mg	na22pg
^{3}He(^{3}He,2p)^{4}He	he3he3	^{14}N(p,n)^{14}O	n14pn	^{23}Na(p,γ)^{24}Mg	na23pg
^{3}He(α,γ)^{7}Be	he3ag	^{14}N(p,α)^{11}C	n14pa	^{23}Na(p,n)^{23}Mg	na23pn
^{4}He(αn,γ)^{9}Be	aang	^{14}N(α,γ)^{18}F	n14ag	^{23}Na(p,α)^{20}Ne	na23pa
^{4}He($\alpha\alpha,\gamma$)^{12}C	aaag	^{14}N(α,n)^{17}F	n14an	^{23}Na(α,n)^{26}Al^{g}	na23an
^{6}Li(p,γ)^{7}Be	li6pg	^{15}N(p,γ)^{16}O	n15pg	^{23}Na(α,n)^{26}Al^{m}	na23an
^{6}Li(p,α)^{3}He	li6pa	^{15}N(p,n)^{15}O	n15pn	^{23}Na(α,n)^{26}Al^{t}	na23an
^{7}Li(p,γ)^{8}Be	li7pg	^{15}N(p,α)^{12}C	n15pa	^{24}Mg(p,γ)^{25}Al	mg24pg
^{7}Li(p,α)^{4}He	li7pa	^{15}N(α,γ)^{19}F	n15ag	^{24}Mg(p,α)^{21}Na	mg24pa
^{7}Li(α,γ)^{11}B	li7ag	^{16}O(p,γ)^{17}F	o16pg	^{25}Mg(p,γ)^{26}Al^{g}	mg25pg
^{7}Li(α,n)^{10}B	li7an	^{16}O(α,γ)^{20}Ne	o16ag	^{25}Mg(p,γ)^{26}Al^{m}	mg25pg
^{7}Be(p,γ)^{8}B	be7pg	^{17}O(p,γ)^{18}F	o17pg	^{25}Mg(p,γ)^{26}Al^{t}	mg25pg
^{7}Be(α,γ)^{11}C	be7ag	^{17}O(p,α)^{14}N	o17pa	^{25}Mg(α,n)^{28}Si	mg25an
^{9}Be(p,γ)^{10}B	be9pg	^{17}O(α,n)^{20}Ne	o17an	^{26}Mg(p,γ)^{27}Al	mg26pg
^{9}Be(p,n)^{9}B	be9pn	^{18}O(p,γ)^{19}F	o18pg	^{26}Mg(α,n)^{29}Si	mg26an
^{9}Be(p,d)^{8}Be	be9pd	^{18}O(p,α)^{15}N	o18pa	^{26}Al^{gs}(p,γ)^{27}Si	al26pg
^{9}Be(p,α)^{6}Li	be9pa	^{18}O(α,γ)^{22}Ne	o18ag	^{26}Al^{ms}(p,γ)^{27}Si	al26pg
^{9}Be(α,n)^{12}C	be9an	^{18}O(α,n)^{21}Ne	o18an	^{27}Al(p,γ)^{28}Si	al27pg
^{10}B(p,γ)^{11}C	b10pg	^{19}F(p,γ)^{20}Ne	f19pg	^{27}Al(p,α)^{24}Mg	al27pa
^{10}B(p,α)^{7}Be	b10pa	^{19}F(p,n)^{19}Ne	f19pn	^{27}Al(α,n)^{30}P	al27an
^{11}B(p,γ)^{12}C	b11pg	^{19}F(p,α)^{16}O	f19pa	^{28}Si(p,γ)^{29}P	si28pg
^{11}B(p,n)^{11}C	b11pn	^{20}Ne(p,γ)^{21}Na	ne20pg		

The references of Sect. 1, 2 and 3 are marked as "intro" in the reference list.